Hindawi
Advances in Materials Science and Engineering
Volume 2022, Article ID 5367695, 16 pages
https://doi.org/10.1155/2022/5367695

Research Article

Fracture Analysis of Compressor Impellers in Olefin Units: Numerical and Metallurgical Approach

Mojtaba Esmailzadeh,[1] Maryam Delshah,[2] Seyedeh Mina Amirsadat,[2] Ahmad Azari,[2] Rouhollah Fatehi,[1] Mohsen Rezaei,[3] Hasan Bazai,[2] Farhad Ghadyanlou,[4] Amir Saidizad,[4] and Mohsen Sharifpur[5,6,7]

[1]*Department of Mechanical Engineering, Faculty of Engineering, Persian Gulf University, Bushehr 75169-13817, Iran*
[2]*Department of Chemical Engineering, Faculty of Petroleum, Gas, and Petrochemical Engineering, Persian Gulf University, Bushehr 75169-13817, Iran*
[3]*Department of Mechanical Engineering, Faculty of Engineering, Shiraz University, Shiraz, Iran*
[4]*R&D Process Engineer, Morvarid Petrochemical Company, Shiraz, Iran*
[5]*Department of Mechanical Engineering, University of Science and Culture, Tehran, Iran*
[6]*Department of Mechanical and Aeronautical Engineering, University of Pretoria, Pretoria 0002, South Africa*
[7]*Department of Medical Research, China Medical University Hospital, China Medical University, Taichung, Taiwan*

Correspondence should be addressed to Ahmad Azari; azari.ahmad@gmail.com and Mohsen Sharifpur; mohsen.sharifpur@up.ac.za

Received 28 October 2021; Revised 17 January 2022; Accepted 1 February 2022; Published 17 March 2022

Academic Editor: Dimitrios E. Manolakos

Copyright © 2022 Mojtaba Esmailzadeh et al. This is an open access article distributed under the Creative Commons Attribution License, which permits unrestricted use, distribution, and reproduction in any medium, provided the original work is properly cited.

This paper presents a failure analysis conducted in 7175 aluminum alloy compressor impellers used in olefin units which operate at 34500 rpm to compress gas in the process. Some characterizations such as chemical composition, microstructure, and hardness tests were conducted to obtain a detailed evaluation of the base alloy. Furthermore, a finite element method and a 3D point cloud data technique have used to determine critical stress points on the surface of impellers. The finite element result showed the root of blades has significant stress concentration. Moreover, the formed cyclic tension has led to a fatigue phenomenon in the root of the blade, so near this location, the local strain accumulation was visible in 3D points cloud data. The fractography results showed that the mode of crack progression and the fractured surface would change by changing the stress mode. In addition, CFD modeling for investigating the effect of flow hydrodynamics on the HP and LP compressor blades is analyzed. The results revealed that the maximum pressure of gas stream for the rotor speed of 34500 had taken place in the area of a blade that already breakdown took place, and the changes of pressure, stress, and temperature gradients of flow in the HP compressor were significantly higher than the LP compressor.

1. Introduction

Compressor is one of the vital equipment in petroleum, chemical, and natural gas industries. On the other hand, the impeller is the most critical part of a compressor. So, the failure of the impeller can impose heavy losses on a system. Depending on the compressor type, the rotational speed of the impeller can reach 2000 to 100000 rpm. There are some methods and tools to study the reasons for impellers failure and the examination of compressor performance. The combination of the numerical optimization technique with the computational fluid dynamics (CFD) is a practical tool to study compressor performance [1]. One of the most important phenomena which usually takes place in the compressors is the formation of liquid droplets. The liquids can have numerous impacts on the surface of impellers due to the velocity of the stream, and the liquid droplets can impose a huge impingement on the impeller of the compressor [2].

Some studies show the effect of droplet impingement on the performance of compressors. For example, Surendranand and Kim [3] carried out research that the purpose of the study was to investigate the effects of liquid droplets on the flow field of a centrifugal compressor stage numerically. Degendorfer et al. [4, 5] carried out numerical and experimental research on the compressor blades; the results indicated that the unsteady forces throughout the operation of the compressor could result in destructive phenomena named resonance response, which can push forward compressor into fatigue cycle. Hong-Li et al. [6] investigated rotor dynamic behavior of turbo-expander involving droplet impact. Since the size and location of the droplets are not known precisely, a stochastic model with beta distribution and Bernoulli distribution has been developed, and the forces resulting from droplet formation have been formulated. The droplet that impacted the impeller blade can lead to a crack in the surface. After that, the stress caused by the rotational velocity in the vicinity of the cracked area can be altered. Therefore, this can decline the performance of the system and also causes breaking down of blades in low temperatures. Consequently, they resulted that the number of channels and blades must be reduced to prevent impeller fatigue. Hundseid et al. [7] evaluated a hydrocarbon multiphase flow, performance parameters, and a wet gas performance analysis. Their results clearly demonstrate that liquid properties greatly impact compressor performance. Since different loads such as centrifugal loads, exciting loads, and aerodynamic loads are applied, impeller work under the hard conditions that include cyclic and dynamic loads. Based on working conditions, impellers are made of different materials such as titanium alloys, stainless steel, and aluminum alloys. Load types, temperature, medium, material, structure, and processing technology are examples of effective factors in the fracture of impeller blades. Accordingly, different mechanisms have been identified as causes of failure of the impeller blades, with fatigue as one of the most common. Because of the high strength and low density of the 7xxx series of Aluminum alloys, these materials have been used to fabricate impellers. However, there are numerous reports of the failure of aluminum impellers fatigue, the dominant mechanism in these failures [8–11]. To evaluate the failure of impellers, the stress distribution should be obtained. Furthermore, the microstructure, machining and final geometry should be investigated carefully. Due to the operating condition of the impeller, it is practically impossible to measure the stress distribution of the impeller blades. However, the stress distribution of the impeller blades can be predicted by finite element analysis (FEA) [8]. Accordingly, the critical positions of the impeller will be identified clearly. The exploitation of this technique can be beneficial in fracture analysis. The combination of the numerical optimization technique with the computational fluid dynamics (CFD) calculation was used to study the correlations between the parameters of geometry and the compressor performance [1]. However, the role of the microstructure of the alloy should be considered in all cases. Azevedo et al. [9] have claimed that the fatigue cracks have initiated from small defects such as impurities. Also, inclusions are suitable stress concentration sites for nucleation of fatigue crack [10]. The inclusions can be the result of the introduction of impurities or various additives during the production process of impellers. Due to the substantial difference between inclusions and base metal, stress concentration can be formed in the interface. Therefore, the microstructure of materials is the most effective factor in fatigue life [10–15]. Yu et al. [11] reported that defective casting process caused shrinkage cavities in the microstructure, which are the stress concentration during loading, and ultimately leads to preimpeller failure. Troshchenko and Prokopenko [12] studied the effects of manufacturing residual stresses, surface defects, and nonmetallic inclusions on fatigue behavior of steels and a titanium alloy. They claimed that there is a complex relationship between the impact of various factors on fatigue strength. It has been verified by many researchers that poor machining can also cause stress concentration sites and the onset of fatigue cracking [11, 13]. Also, the heterogeneous structure, such as welded joint, can be a site of stress concentration and reduce the fatigue life of the impellers [12, 13]. A 3-dimensional (3D) point cloud is a new technique that has found lots of applications in reverse engineering recently. It has been used to prepare 3D drawings of engineering parts with high accuracy [13]. Studies have shown that 3D point cloud data has sufficient accuracy in extracted pipe spools [14] and cylinders and estimation of their parameters [15]. Therefore, it is useful for comparing the geometrical changes that occurred before and after servicing the pieces. Wang et al. [13] reported that (3D) point cloud be used as a new technique for geometry quality inspection in a review article. However, the application of this technique is more in the field of reverse engineering than geometry quality inspection.

The literature has shown that the systematic investigation of the failure mechanism of impellers has not been carried out. So, in this study, three fractured impellers have been analyzed to determine the cause and mechanism of failure using CFD, finite elements (FE), and metallurgy analysis.

2. Materials and Method

2.1. Metallurgical Analysis. Three compressor impellers were selected for this study to evaluate fracture analysis. All working conditions were similar, but the service life was varied. The code and the lifetime of each sample have been listed in Table 1. The impellers were designed and fabricated by various companies. In fact, to choose the best product from different companies, random samples from each company have been selected for investigation. The standard composition of 7175 Al alloy was extracted from ASM handbook volume 2. However, all impellers failed in less than the designed time. Figure 1 shows three fractured impellers, samples 1, 2 and 3, respectively. The diameter of all impellers was 16 cm. All fracture points and then the critical points of the fracture zone were cut, and microscopic evaluation was performed on them. Table 2 represents the chemical composition of samples. This test was

Table 1: Lifetime of specimens.

Sample	Life time (day)	Condition
1	240	HP compressor
2	180	HP compressor
3	120	HP compressor

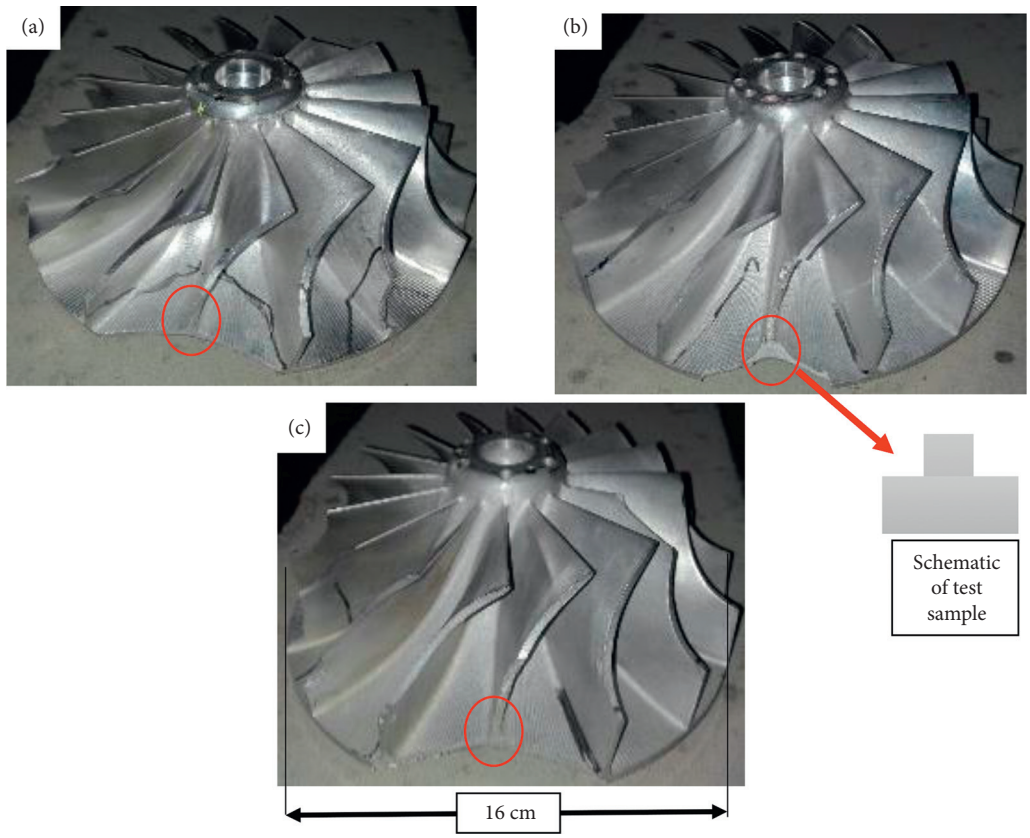

Figure 1: Three fractured impellers and schematic of test sample for (a) sample 1 (b) sample 2 (c) sample 3.

Table 2: Chemical composition of specimens (%wt.).

Samples	Al	Zn	Mg	Cu	Fe	Si	Cr
1	Bal.	6.42	2.19	1.99	0.204	0.073	0.22
2	Bal.	6.252	2.202	1.956	0.254	0.060	0.222
3	Bal.	6.848	2.166	1.079	0.138	0.064	0.198
Standard	Bal.	5.1–6.1	2.1–2.9	1.2–2	0–0.2	0–0.15	0.18–0.28

performed with a spectroscopic device (SOLARIS ccd plus model). The base metal of impellers was evaluated by microstructure, phase characterization, and hardness tests. Metallographic specimens were prepared by cutting, grinding, mounting, and sanded using 180–3000 mesh sandpapers, and polished by special felt, followed by etching in a solution that contained 95 ml distilled water, 2.5 ml HNO_3, 1.5 ml HCl, and 1.0 ml HF, and the duration of etching was 6–9 seconds. Optical microscopy (OM) and scanning electron microscopy (SEM TESCAN-Vega 3) equipped with energy-dispersive X-ray spectroscopy (EDS) analysis system were applied to characterize microstructure. The phases of microstructure were identified by X-ray diffraction (XRD) method. The prepared specimens were inserted into the Philips X'Pert PW 3040 device to accomplish this test. The XRD test was performed at a scan rate of 0.05 degrees.

Furthermore, the Brinell hardness (HB) was measured on all specimens at least three times as well as before and after service at a load of 500 kg. Fractured surfaces were examined by an ordinary camera and above mentioned SEM to identify the location of the cracking initiation and the

failure mechanism. In addition, 3D scanner equipment was used to obtain point cloud data from specimens before and after service. Evaluation of the deformation behavior of the blades of the impeller was the primary purpose had been the results of this technique. For this experiment, Steinbichler 3D scanner set-up was used.

2.2. Numerical Analysis. The procedure was divided into four steps for numerical simulation of the flow inside the compressor blade. In the first step, the CAD model of the mentioned blade was generated. Figure 2 and Table 3 indicate the CAD model of the blade with boundary conditions and the dimensions of the model, respectively. In the second step, the computational domain to discretize equations has been prepared that is shown in Figure 3. All the discretized equations have been solved by using a CFD code at the third step. FVM numerical approach has been employed to solve governing equations. A second-order upwind scheme was applied for discretizing the momentum equation, turbulence equation, and energy equation on the provided grid. The SIMPLE algorithm has been considered for Pressure-Velocity coupling. Also, a steady state rotating reference frame (RRF) handles the rotation of the wheel of the compressor. The final step of the modeling was post-processing of the outcomes from CFD computations which have been analyzed and compared with the experimental results to evaluate the blade fatigue. The information of both computational grids and models has been provided in Tables 3 and 4, respectively.

For FEM analysis, the boundary and loading conditions were considered as follows:

The effect of the centrifugal field was modeled as a volumetric force, which extends from the center of the rotating body to the outside. The rotating field was designed for 34500 rpm angular velocity in static modeling.

The loading due to fluid flow was modeled as the pressure difference between the two sides of the blades. This loading was applied to the blade surfaces as compression.

Since the blade was moving at a constant angular velocity, the effect of centrifugal force was applied to it in the form of a field, and the problem was static requiring boundary conditions of fixed support on the part connected to the shaft.

3. Results and Discussion

3.1. Fractography. In Figure 1 schematic of the test sample is shown. In continue, its macrostructure can be seen for sample 3 in Figure 4. This fatigue fracture surface illustrates different regions that include: S (Stage I) A and B (stage II), and C (ductile fracture). The red arrows indicate crack directions. The crack initiated in S and branched to A and B regions. The plastic accumulation method [16] is dominant in the B region, and this area has undergone shear deformation. In contrast, the dislocation blockage mechanism is predominant for region A and a different fracture surface is created than in region B. Therefore, region A shows the mussel-like surface or so-called fatigue-induced beach marks and region B illustrates shear dimples. The region C indicates final fatigue fracture with brittle fracture surface. Fatigue crack in zones A and B have reached its critical size. Finally, the C region has formed abruptly and rapidly in the last step and completed the fatigue failure.

In all specimens, fatigue crack initiated at the surface and propagated with different paths. Figure 5 illustrates high magnification of the initiation crack site (S region in Figure 4) for samples 1 and 3. In addition, it can be seen different cracks in this subsurface area.

Figure 6(a) shows the high magnification of Zone A with beach marks. In zone A, the direction of crack propagation has been perpendicular to the direction of load and beach line marks. This pattern is quite common for fatigue failures. In this zone, the crack tip undergoes plastic deformation and progresses slowly. In general, the cracks propagate in the perpendicular direction of the highest tensile stress [17]. A comparison of Figures 6(a) and 6(b) indicate that the crack progressive was different in the two regions (A&B). In fact, the crack direction has angularity with applied tension mode in the B region. For this reason, deformed dimples are noticeable in region B. In addition, the EDS results confirm the presence of coarse Al_2MgCu precipitations in this area.

Given the geometry of blades and hub connection, it seems that the critical crack length was about 2 mm. This area is shown in Figure 6(a) by a yellow dashed line.

3.2. Metallurgical Characterization. Figure 7 shows OM images of all specimens. Sample 2 has more recrystallization microstructure than others, but the average size of the precipitations of sample 2 is higher than both samples 1 and 3. Also, it can be seen that all microstructures have been overaged. The more magnification of microstructure of sample 2 is illustrated in Figure 7(d). This phenomenon is confirmed clearly by the presence of precipitations in the grain boundaries. Arrows in Figure 7 indicate some of them. It was mentioned that this alloy is susceptible to overageing [18].

The EDS results of the grain boundary precipitation have been illustrated in Figure 8. It can be seen that Al_2MgCu (S phase) precipitation has formed in the grain boundary. This phase has a centered-orthorhombic crystal structure [19]. Also, this precipitation on a large scale can be the site of crack initiation under loading. This phenomenon is displayed in Figure 9 for one precipitation in sample 3. In other words, the clear discontinuities (yellow arrows) are visible between precipitation and Al alloy matrix. It should be noted that this image was created without the etching process. Comparison of the different samples showed two points: the number of precipitations varies for different specimens and severe precipitations discontinuity with the Al matrix in sample 3. Although low deposition of this precipitate can improve the mechanical and corrosion properties [20], increasing the amount of this precipitate has the opposite effect on the mechanical properties. The existence of the latter precipitations is one of the significant weaknesses of this Al alloy microstructure. Moreover, Al grain boundaries may have been embrittled by large S phase precipitation. It

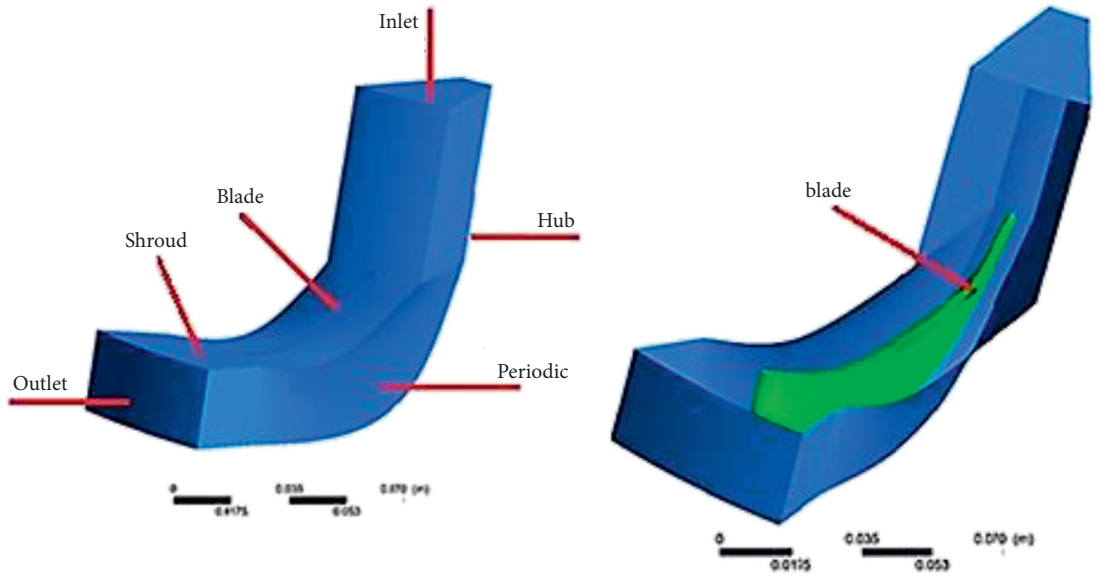

Figure 2: (a) Geometry of a compressor row with boundary conditions (b) Geometry of a compressor row with the blade.

Table 3: Compressor blade geometry information.

Number of blades	16
Inlet cross-sectional area (m^2)	0.0011
Outlet cross section (m^2)	0.0013
Inlet hydraulic diameter (m)	0.0304
Outlet hydraulic diameter (m)	0.0336

Table 4: Information on grid computation model.

Number of elements	104545
Minimum orthogonal quality	0.64
Maximum skewness	0.36
Maximum aspect ratio	10.39

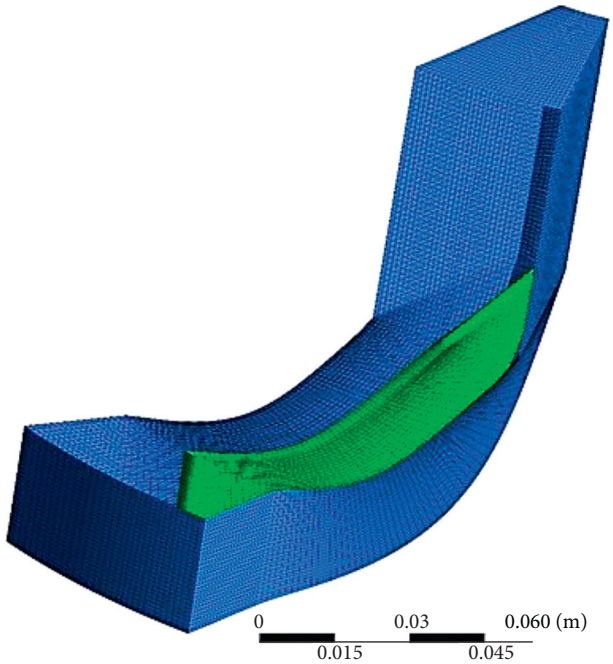

Figure 3: Mesh for a blade of compressor with fluid around it.

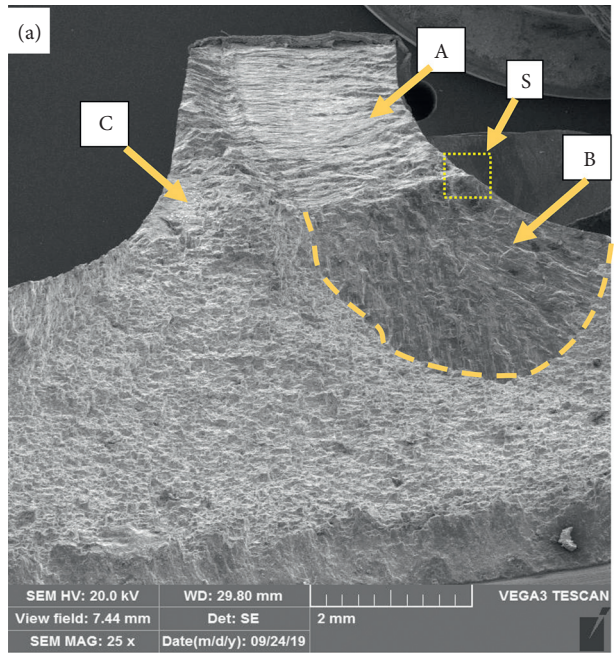

Figure 4: Macrostructure of fracture surface for sample 3.

can be seen large cracks between precipitation and Al matrix in Figure 9. The main reason of this phenomenon is related to the incoherency of precipitation. According to Chen et al. [21], the coherency degree of the precipitates with the 7055 Al alloy is the main factor in the fatigue crack progressive. In the present work, the crack growth rate was very high due to

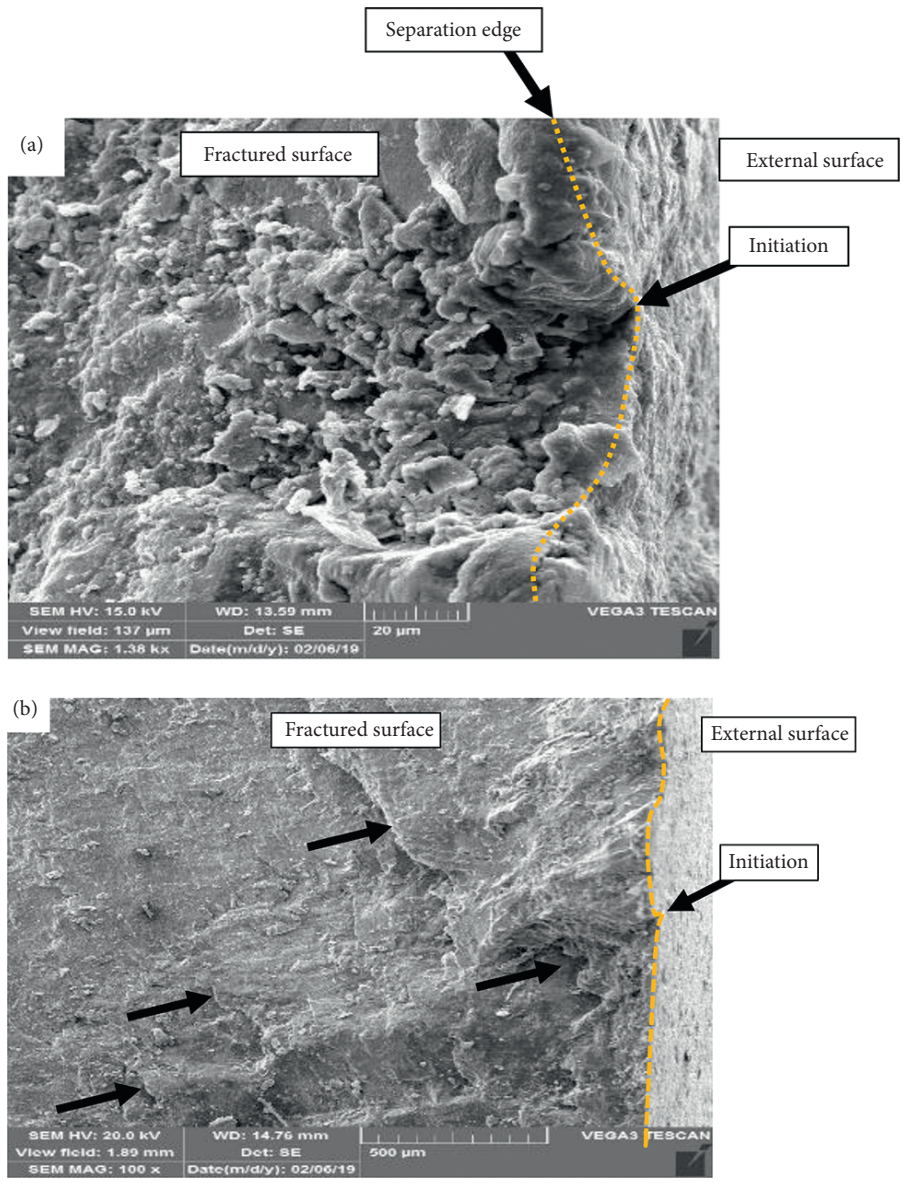

Figure 5: SEM fractured surface of S region in Figure 4 (a) sample 1 (b) sample 3.

low coherency between precipitations and Al matrix (Figures 8 and 9).

According to Table 2, specimens have a close chemical composition close to 7175 Al standard composition, such as ASTM B227. This alloy should have at least 1.2%wt Cu according to this standard. Specimen 3 has a lower Cu in its composition. Due to the role of Cu element in the strength of this alloy, it was expected that this sample would exhibit weaker mechanical properties. Lim et al. [22] claimed that the amounts of Zn, Mg, and Cu have a decisive role in the formation of reinforcing phases and affect the strength of 7175 Al alloy. The XRD result of the samples is shown in Figure 10. It should be noted that excessive amounts of Cu can also lead to the formation of the destructive S phase (Al_2MgCu). Therefore, sample 3 was expected to have the least amount of destructive S phase. But this is not an accurate conclusion. Because the phase formation depends on the heat treatment applied in addition to the chemical composition.

The results of the hardness test are shown in Table 5. The hardness of all samples is lower than the standard limit of 7175 Al alloy (152 HB). It can be seen that samples 1 and 3 have the highest and lowest hardness, respectively. The coarsening of S phase precipitations was the main cause of this result. A comparison of the number and size of S phase precipitations between different specimens has shown that sample 1 has better conditions due to the microstructure of sample 1 has a uniform distribution of precipitations. In other words, the uniform distribution of fine precipitations resulted in higher Brinell hardness. However, it should be reminded that all samples have been over-aged. Therefore, the distribution of precipitations is another main factor in fatigue strength. The same results were reported by Kobayashi et al. [23] for 20–11P steel alloy.

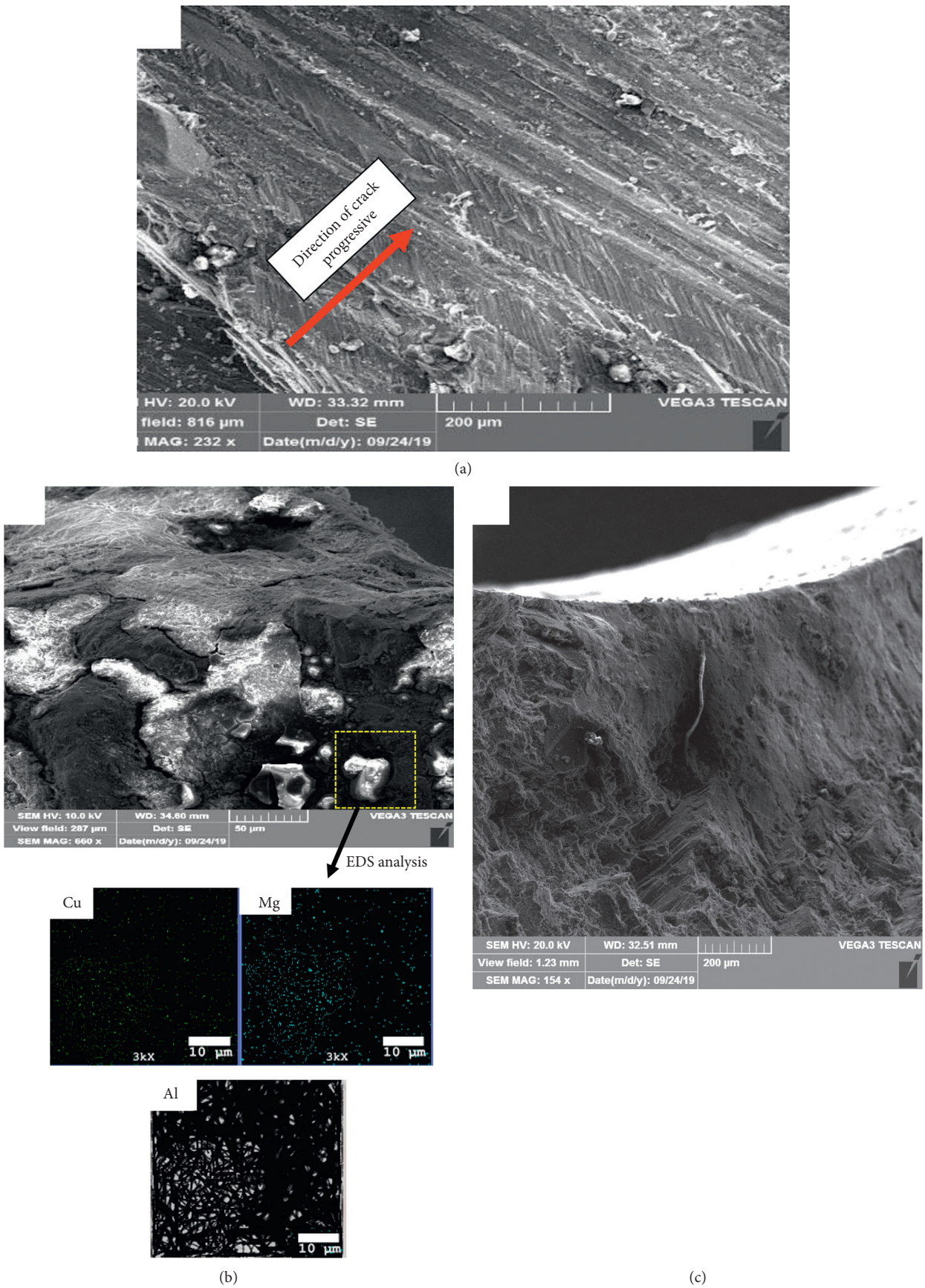

Figure 6: SEM image of fractured surface of sample 3 (according Figure 4) (a) zone A (b) zone B and (c) zone C.

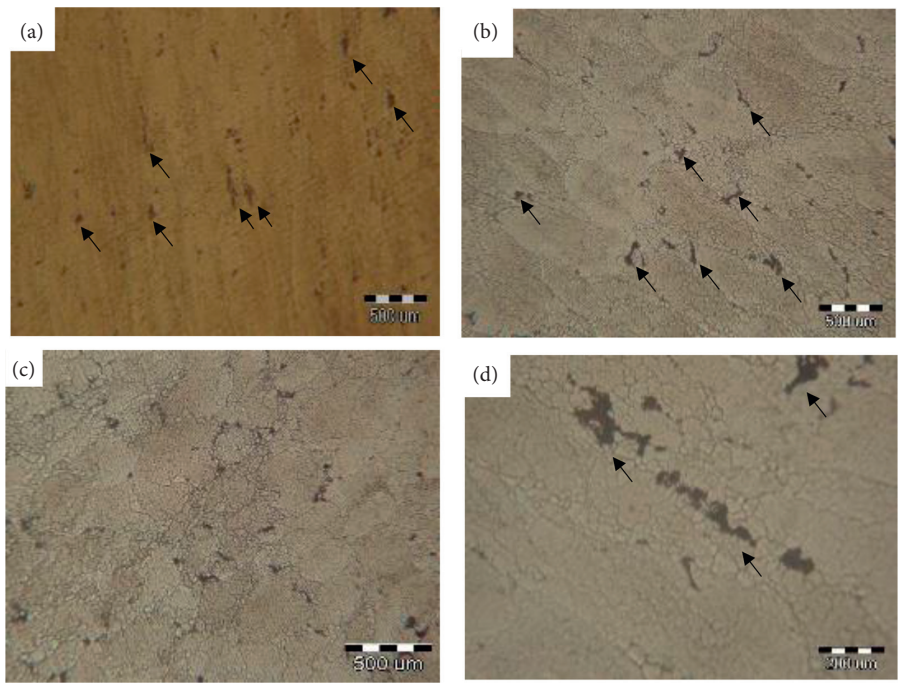

Figure 7: OM images of microstructure of (a) sample 1 (b) sample 2 (c) sample 3 (d) higher magnification of sample 2.

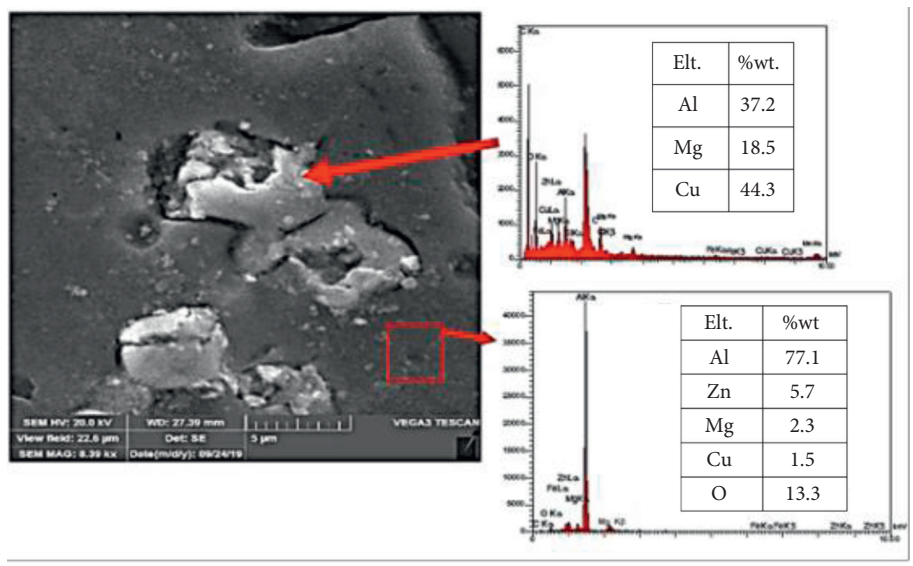

Figure 8: SEM& EDS results of grain boundary precipitation (sample 1).

3.3. Finite Element and Numerical Analysis. Figure 11 shows the result of the CFD simulation for HP and LP Compressor. The results revealed that the maximum pressure of the gas stream for the rotor speed of 34500 rpm has taken place in the fractured area of the blade. The shear stress (WSS) contours are shown in Figure 12, which also indicates the maximum in the breakdown zone. The temperature gradient for HP and LP Compressor is shown in Figure 13. In addition, fluid velocity vectors in a row of the compressor from the inlet to the outlet are shown in Figure 14. The results showed that the pressure, stress gradients on the HP blade were significantly higher than the LP compressor, providing the reason for the blade fracture in the HP compressor.

The parametric geometry model of the impeller was made according to technical drawing using ANSYS software.

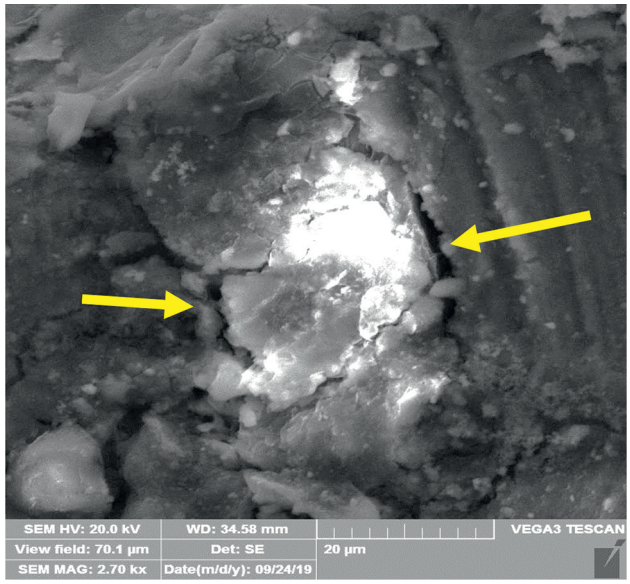

Figure 9: SEM image of grain boundary precipitation and cracks (sample3).

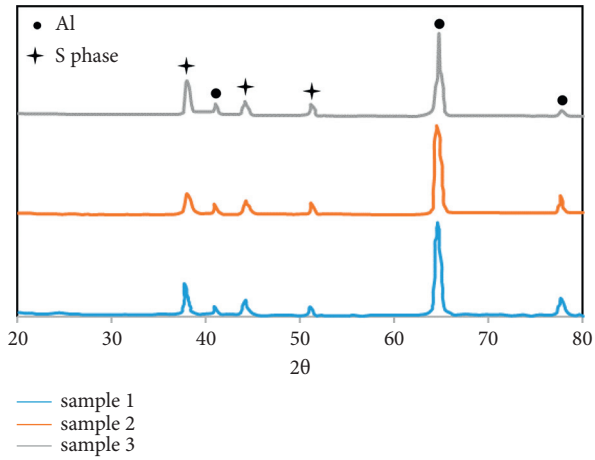

Figure 10: XRD results of all specimens.

Table 5: Brinell Hardness test.

Samples	Brinell 500			HB 500 ave.
	No.1	No.2	No.3	
Sample 1	148.3	147.6	149.4	148.4
Sample 2	144.2	145.4	144.9	144.8
Sample 3	139.2	139.8	140.5	139.8

The final model of the impeller consisted of 114600 nodes and 125101 elements for one blade. As already mentioned, the impeller of the compressor endures a combination of centrifugal and surface loads [24, 25].

3.3.1. Validation. To evaluate the results of CFD simulation, the industrial data was provided by the R&D Unit of Morvarid Petrochemical Company (MPC) has been used, and for both LP and HP the same impeller has been used. According to Table 6 the boundary condition which was set up for both inlet and outlet were kind of constant pressure named pressure-inlet and pressure-outlet, respectively. Therefore, after model convergence to validate the model results, the calculated mass flow rate from the CFD simulation was compared to the actual mass flow. Table 7 shows the comparison of the simulation results and the industrial results of HP and LP compressors. As can be seen from the obtained results, there is a good agreement between the results of modeling and the operational results of the process, which indicates the accuracy of the modeling.

The surface load is caused by gas fluid pressure. Figure 15 illustrates the contour of the total deformation of the impeller at 0.1 bar pressure difference in 34500 rpm. The value of pressure difference was extracted from process conditions. Since the fluid analysis results show that the pressure difference between the two sides of the blade is less than 1 bar, there is no need to transfer the pressure distribution to the structural analysis. Instead, the pressure is applied uniformly to the lower surface of the blade.

Figure 15(a) illustrates that the maximum deformation is about 0.1 mm. The extracted contour of elastic strain and von-Mises stress for mentioned conditions are shown in Figures 15(b) and 15(c), respectively. The extracted contours illustrate the maximum stress has accrued in the root of the blades of the impeller. This is due to the interference of the torque due to the centrifugal force and the fluid pressure, which is maximized at this point. Moreover, Von-Mises stress has a maximum value of 231 MPa in the root of the blades of the impeller. This phenomenon is evident in Figure 16.

In the following, to estimate the effect of the maximum fluid pressure and make the more critical situation with respect to the actual situation, the pressure difference was increased to 0.5 bar, and the calculations were repeated. The results of the latter state have illustrated in Figure 17. In this state, the maximum total deformation was 0.45 mm on the tip of the blades. It seems the fluid pressure has predominated to centrifugal load in this location. However, the root of the blades has maximum stress of 249 MPa in Figure 18. Therefore, due to the high proportion of centrifugal loads, the maximum stress does not increase as the pressure difference increases in the root of blades. The compared results between pressure differences of 0.1 and 0.5 are shown in Table 8. In summation, based on Figures 15 and 17 the location of maximum stress occurs at the root of the compressor blade. For example, for pressure difference 0.5, in Figure 17, the value of Von-Mises stress in the root is in the interval 166–250 MPa, while this value for other parts are below 110 MPa, this difference is considerable. Based on this analysis the probability of failure in the blade's root is much higher than in the other parts.

The fatigue strength on the titanium alloy studied according to the literature [26], for 10^7 cycles is about 200–250 MPa. The present study's maximum stress is between 230 and 250 MPa. The results show an acceptable agreement of the present work with the previous literature.

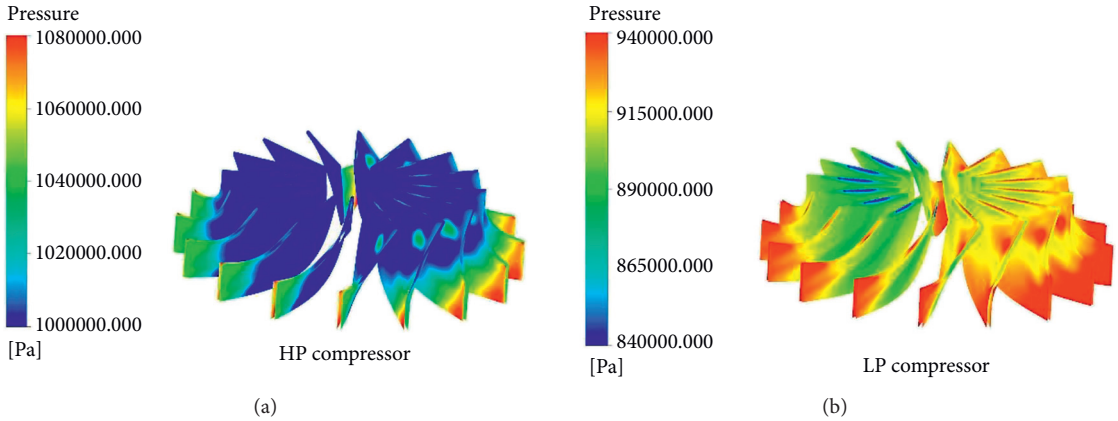

Figure 11: Contour of pressure for (a) HP Compressor (b) LP Compressor.

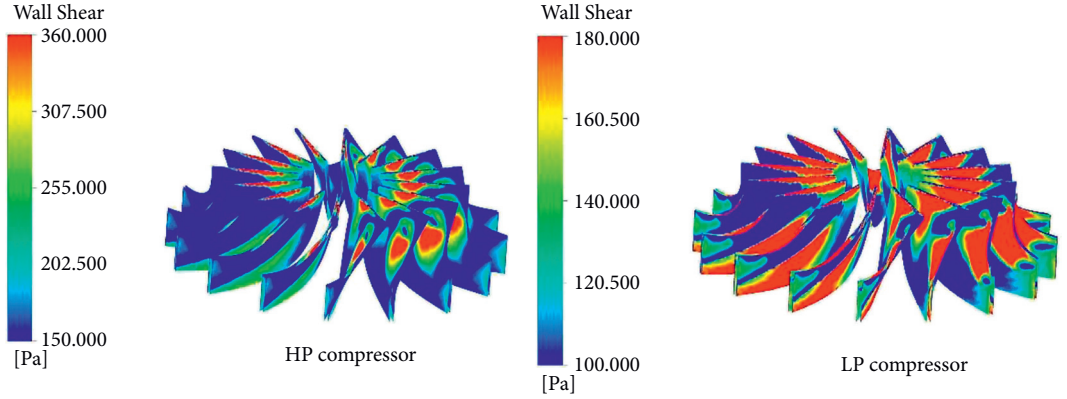

Figure 12: Contour of shear stress for (a) HP Compressor (b) LP Compressor.

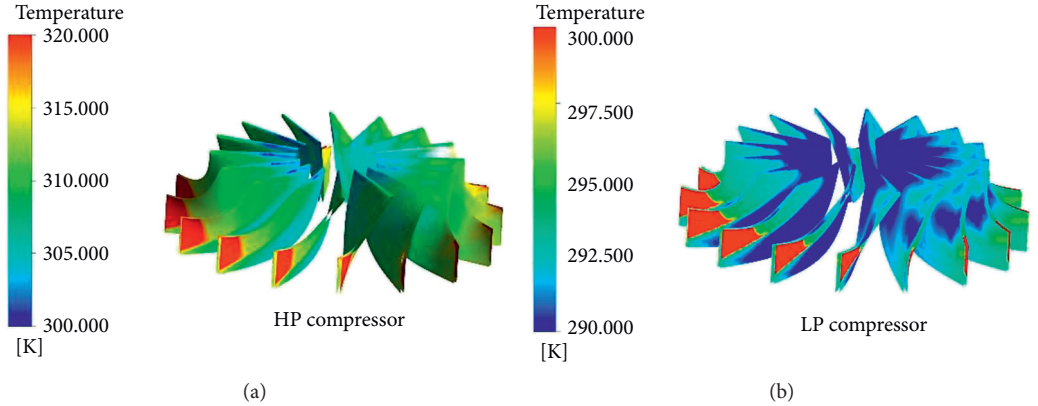

Figure 13: Contour of temperature for (a) HP Compressor (b) LP Compressor.

3.4. 3D Points Cloud Technique. Figure 19 shows traditional camera photos of samples before and after service. Since the original sample was the basis for preservice parts verification, it has been avoided to reproduce the preservice photos of samples 2 and 3 in Figure 19. It can be seen that all specimens undergo local deformation near the blade to hub junction. This site is near the fractured surface on the ruptured blade. It can be concluded that discontinuities accumulated at this position. This means that deformation bands are formed by applying a large external load at the concentration stress sites due to asymmetric slippage of the crystal planes. With the formation of deformation bands, crystalline defects such as voids move in the same direction to accumulate at the point of crack initiation. Therefore,

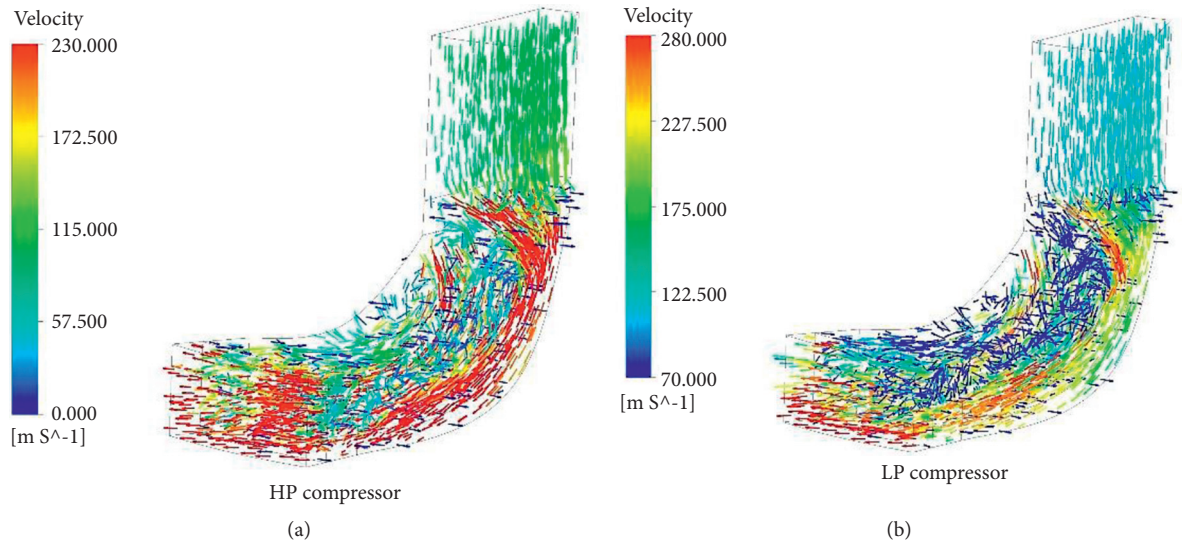

Figure 14: Velocity vector for (a) HP Compressor (b) LP Compressor.

Table 6: Information on boundary conditions and models.

Inlet mass flow rate (kg/s)		0.1994
Inlet temperature (K)		306.65
Inlet pressure (kPa)		842
Outlet temperature (K)		322.65
Outlet pressure (kPa)		969
Diameter of liquid droplets (m)		250×10^{-6}
Mole fraction of the components	Methane	0.5483
	Ethane	0.0068
	Ethylene	0.0227
	Carbon monoxide	0.0113
	Hydrogen	0.4169

Table 7: Comparison of simulation results with compressor operating results at rpm 34500 rpm.

	Outlet mass flow (kg/hr) HP compressor	Outlet mass flow (kg/hr) LP compressor
Simulation result	10600	11065
Industrial result	11490	11490
Error	7.7%	3.6%

microcracks develop easily in stress concentration sites. On the other hand, the size of these microcracks depends on the microstructure of the material and the concentration of stress due to the external load. The same result has presented by Affonso [17]. In this stage, the crack is tiny and unobservable with an unaided eye.

The 3D points cloud technique was used for exact investigation of deformation of all sections of compressor impellers after service. Figure 20 illustrates 3D images of sample 3 before and after service with high magnification. The 3D image of sample 3 is analyzed before and after service for better comparison. It can be seen that deformation is the highest near the junction of the blade and hub of the impeller. So that the radius of the connection of the blade to the hub has changed from 6 mm to 5.9 mm for sample 3. This change was lower for samples 1 and 2. As the radius becomes smaller, the stress concentration at this point will increase. Therefore, this technique can well show small geometric changes, especially for critical points of the impeller. According to the cyclic load system and fatigue condition for impeller blades, accumulation of elastic strain lead to local plastic deformation in this site. Due to the presence of coarse precipitations in the grain boundaries of crystalline structure, elastic strains have accumulated around them. Recently, Malitckii et al. [27] reported the strain accumulation during microstructurally small fatigue cracks by the digital image correlation technique. Therefore, given the over-aged microstructure (coarse precipitations), sufficient conditions have been provided for a new impeller fracture surrounding the blade-to-hub connection area.

On the other hand, the presence of stress concentration can accelerate the crack initiation step. Accordingly, large

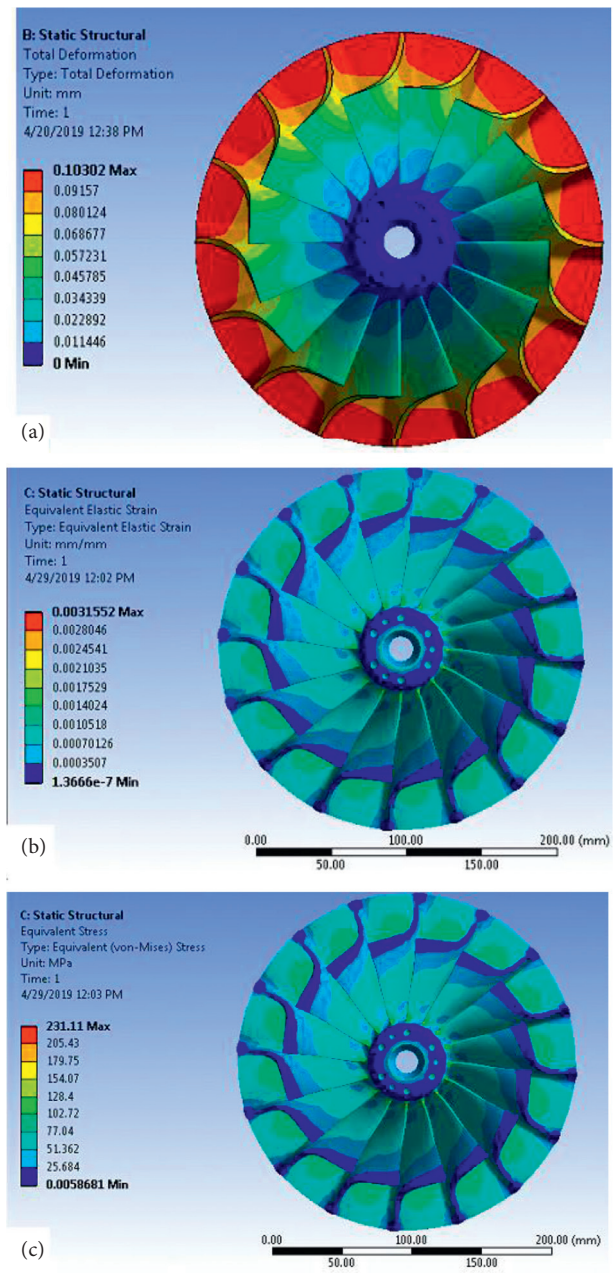

Figure 15: The extracted contour of (a) total deformation (b) elastic strain (c) Von-Mises stress for pressure difference 0.1 bar in 34500 rpm.

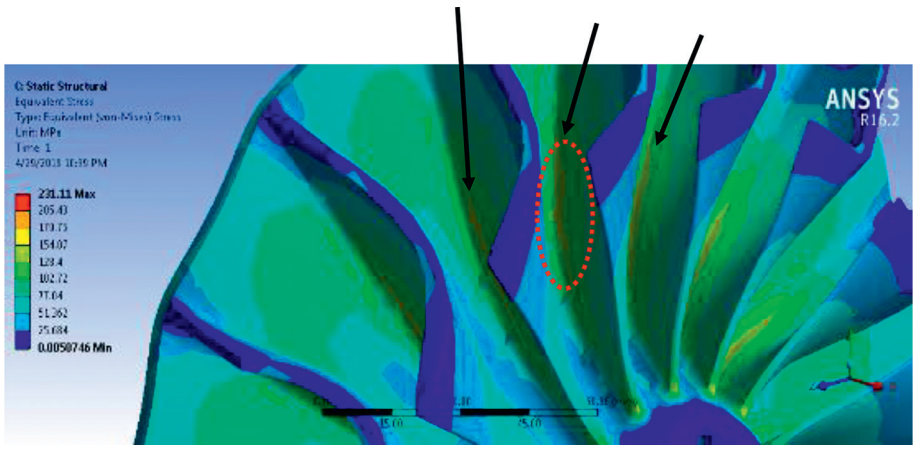

Figure 16: High magnification of The contour of Von-Mises for 0.1 pressure difference in 34500 rpm.

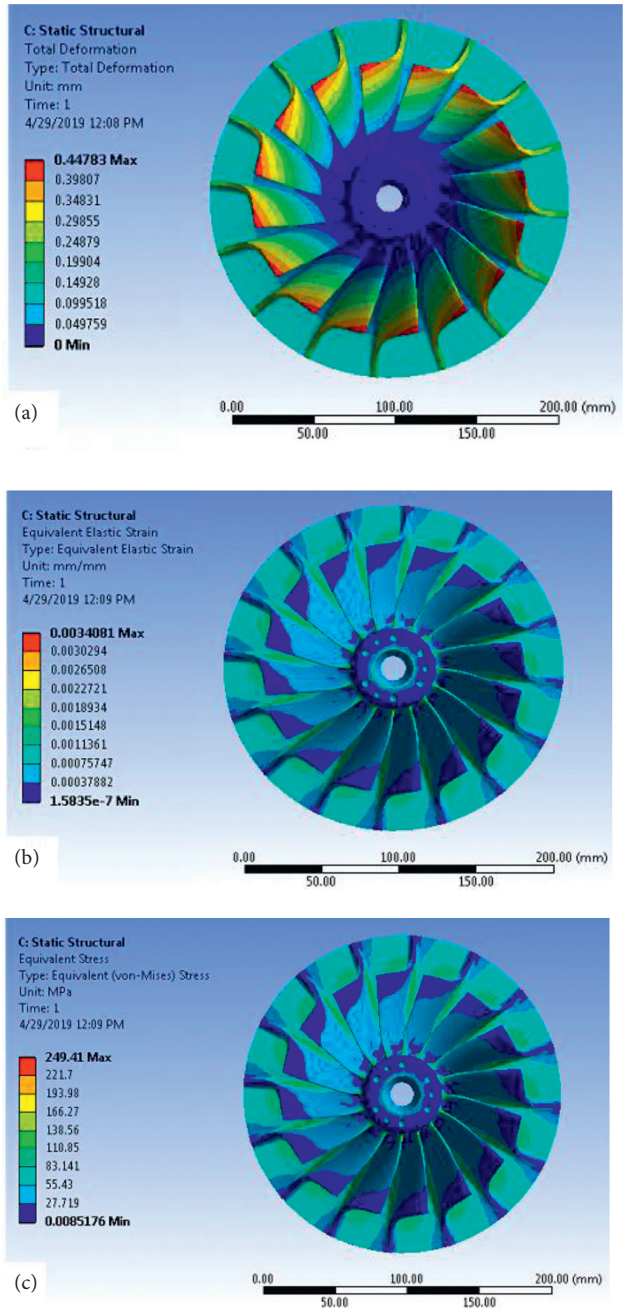

Figure 17: The contour of (a) total deformation (b) Elastic strain (c) Von-Mises stress for pressure difference of 0.5 bar in 34500 rpm.

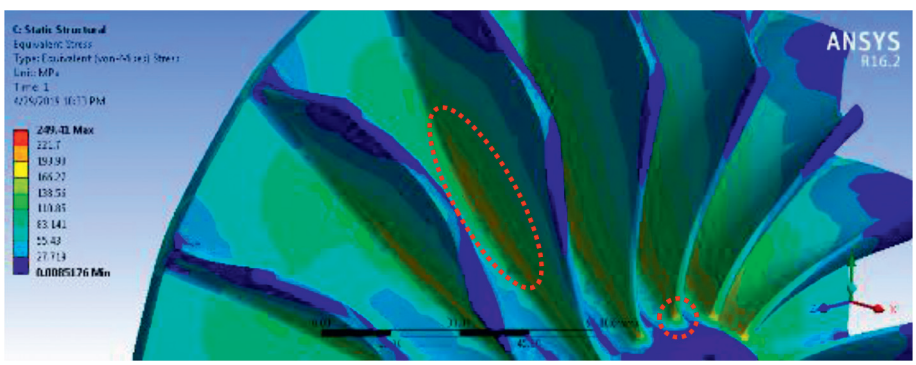

Figure 18: High magnification of the contour of von-mises for pressure difference of 0.1 in 34500 rpm.

Table 8: Compered FEM results between pressure difference 0.1 and 0.5.

Pressure (bar)	Von-mises stress (MPa)	Equivalent elastic strain	Deformation (mm)
0.1	231.1	0.003155	0.1030
0.5	249.4	0.003440	0.4473

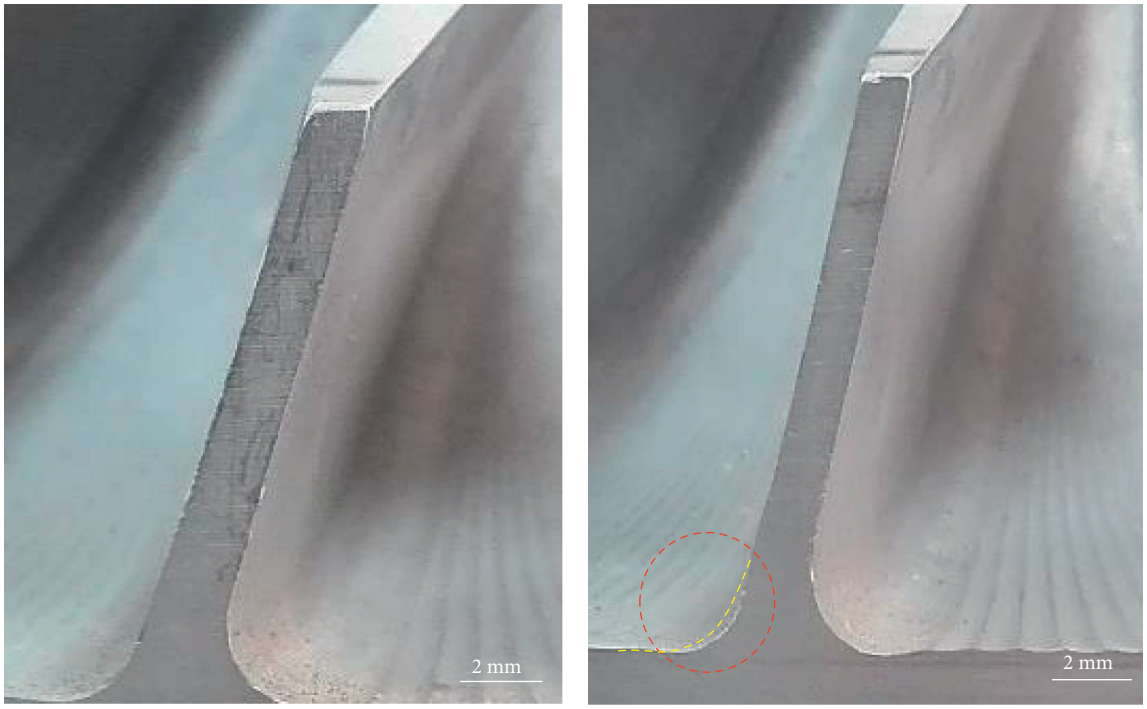

(a) (b)

Figure 19: Camera image of sample 3 (a) before service (b) after service.

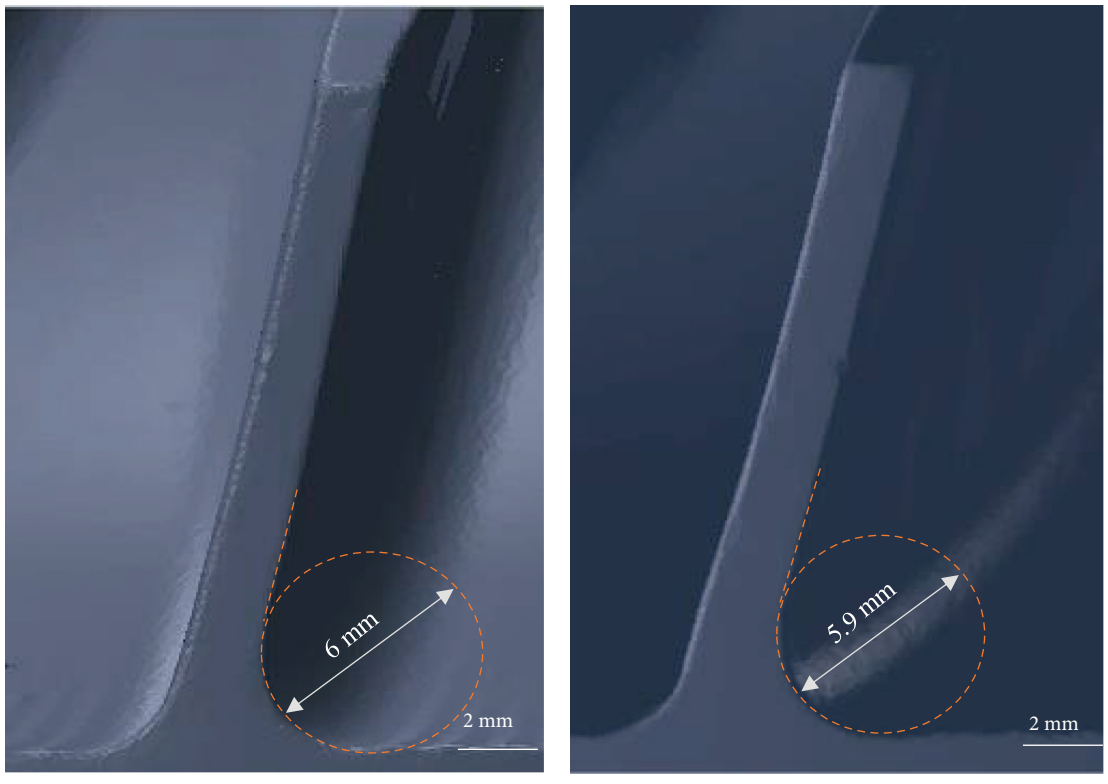

(a) (b)

Figures 20: 3D points cloud of sample 3 (a) before service (b) after service.

precipitations have accelerated the fatigue crack formation in all three samples. The same result has reported for AA2524-T3 alloy [28].

In general, some design features may act as stress concentration sites such as fillets between blades and hubs on impellers. Also, all investigated impellers have inappropriate microstructure causing intergranular precipitations. All these factors led to the fatigue failure of the junction of the blade to the hub of impellers. Depending on the number and distribution of precipitations, the service life varies from sample 1 to 3, maximum to minimum, respectively. The same results have been reported by Moreira [29] for AA 2618 T652 alloy compressors wheels. However, the impellers were in a corrosive environment in their samples, and this degradation was more severe.

4. Conclusion

The failure impellers were operated at 34500 rpm. The initial evaluation indicated a similar failure mode for all specimens. The simulation of impeller service showed stress concentration in some regions of the impeller, such as the root of blades, and 3D points cloud technique showed local deformation in impellers.

(1) The phenomenon of fatigue has been the most important factor in the failure of all impeller blades. In addition, inadequate microstructure due to the overageing of 7175 Al alloy has led to premature failure of the blades

(2) The stress due to centrifugal motion has been much higher than fluid stress

(3) It was found that the root of the blades has maximum stress of 249 MPa, which leads to a deformation of 0.45 mm

(4) The radius of curvature of the impeller root has changed by 0.1 mm, and this amount has intensified the stress concentration conditions in this area

(5) 3-D points cloud technique can detect local deformations of the impeller with accuracy and prevent sudden failures with greater degradation in overhaul times

According to the results, it seems that the precise control of the alloy composition and its microstructure can lead to an increase in the service life of the impellers. However, the authors have put another proposal on the agenda to consider other alloys such as Ti–6Al–4V titanium alloy to evaluate its performance in this situation.

Data Availability

The data will be available upon request.

Conflicts of Interest

The authors declare that they have no conflicts of interest.

References

[1] K. Ashihara and A. Gotop. V001T003A053, 2001.

[2] C. V. Halbe, W. F. O'Brien, W. T. Cousins, and V. Sishtla, "A CFD analysis of the effects of two-phase flow in a two-stage centrifugal compressor," in *ASME Turbo Expo 2015: Turbine Technical Conference and Exposition*, American Society of Mechanical Engineers Digital Collection, 2015.

[3] A. Surendran and H. D. Kim, "Effects of wet compression on the flow behavior of a centrifugal compressor: a cfd analysis," in *ASME turbo expo 2014: turbine technical conference and exposition*, American Society of Mechanical Engineers Digital Collection, 2014.

[4] C. Degendorfer, R. S. Abhari, K. Vogel, and R. Hunziker, "Journal of the global power and propulsion society," vol. 2, pp. 415–428, 2018.

[5] U. Haupt and M. Rautenberg, "Blade vibration measurements on centrifugal compressors by means of telemetry and holographic interferometry," *Journal of Engineering for Gas Turbines & Power*, vol. 106, no. 1, pp. 70–78, 1984.

[6] H. Li, M. Li, S. Zhou et al., "Rotor dynamics behavior of turboexpander involving droplet impact," *Mathematical and Computer Modelling of Dynamical Systems*, vol. 22, no. 5, pp. 444–462, 2016.

[7] O. y. Hundseid, L. E. Bakken, T. G. Gru¨ ner, L. Brenne, and T. Bjorge, "Wet gas performance of a single stage centrifugal compressor," *Turbo Expo: Power for Land, Sea, and Air*, vol. 43178, pp. 661–670, 2008.

[8] S. Liu, C. Liu, Y. Hu, S. Gao, Y. Wang, and H. Zhang, "Fatigue life assessment of centrifugal compressor impeller based on FEA," *Engineering Failure Analysis*, vol. 60, pp. 383–390, 2016.

[9] T. F. Azevedo, R. C. Cardoso, P. R. T. da Silva, A. S. Silva, and S. Griza, "Analysis of turbo impeller rotor failure," *Engineering Failure Analysis*, vol. 63, pp. 12–20, 2016.

[10] Y. Zhang, J. Wang, Q. Sun, H. Zhang, and P. Jiang, "Fatigue life prediction of FV520B with internal inclusions," *Materials & Design*, vol. 69, pp. 241–246, 2015.

[11] Z.-w. Yu, X.-l. Xu, and H. Yu, "Fracture analysis of blade of an integrated compressor impeller," *Journal of Failure Analysis and Prevention*, vol. 13, no. 3, pp. 320–327, 2013.

[12] V. T. Troshchenko and A. V. Prokopenko, "Fatigue strength of gas turbine compressor blades," *Engineering Failure Analysis*, vol. 7, no. 3, pp. 209–220, 2000.

[13] Q. Wang and M.-K. Kim, "Applications of 3D point cloud data in the construction industry: a fifteen-year review from 2004 to 2018," *Advanced Engineering Informatics*, vol. 39, pp. 306–319, 2019.

[14] T. Czerniawski, M. Nahangi, C. Haas, and S. Walbridge, "Pipe spool recognition in cluttered point clouds using a curvature-based shape descriptor," *Automation in Construction*, vol. 71, pp. 346–358, 2016.

[15] T.-T. Tran, V.-T. Cao, and D. Laurendeau, "Extraction of cylinders and estimation of their parameters from point clouds," *Computers & Graphics*, vol. 46, pp. 345–357, 2015.

[16] P. Chowdhury and H. Sehitoglu, "Mechanisms of fatigue crack growth - a critical digest of theoretical developments," *Fatigue and Fracture of Engineering Materials and Structures*, vol. 39, no. 6, pp. 652–674, 2016.

[17] L. O. A. Affonso, "Fatigue fractures," in *L. O. A. Affonso (Ed.) Machinery Failure Analysis Handbook*Gulf Publishing Company, 2006.

[18] A. Azarniya, A. K. Taheri, and K. K. Taheri, "Recent advances in ageing of 7xxx series aluminum alloys: a physical

metallurgy perspective," *Journal of Alloys and Compounds*, vol. 781, pp. 945–983, 2019.

[19] S. B. Wang, J. H. Chen, M. J. Yin et al., "Double-atomic-wall-based dynamic precipitates of the early-stage S-phase in AlCuMg alloys," *Acta Materialia*, vol. 60, no. 19, pp. 6573–6580, 2012.

[20] T. Vu Dinh, W. W. Sun, Y. Yue, Y. Wu, C. R. Hutchinson, and S. Thomas, "On the miniaturised sacrificial protection achieved by surface precipitation in aluminium alloys," *Corrosion Science*, vol. 145, pp. 67–79, 2018.

[21] J.-z. Chen, L. Zhen, S.-j. Yang, and S.-l. Dai, "Transactions of nonferrous metals society of China," vol. 20, pp. 2209–2214, 2015.

[22] S. Lim, T. nbsp, I. Eun, nbsp, S. N. Sang, and W. nbsp, "Materials transactions," vol. 44, pp. 181–187, 2003.

[23] M. Kobayashi, M. Yamamoto, and O. Miyagawa, "Effect of precipitation hardening on the fatigue strength," *Bulletin of JSME*, vol. 21, no. 154, pp. 554–560, 1978.

[24] T.-G. Kim and H.-C. Lee, "Failure analysis of MVR (machinery vapor recompressor) impeller blade," *Engineering Failure Analysis*, vol. 10, no. 3, pp. 307–315, 2003.

[25] Q. Chu, M. Zhang, and J. Li, "Failure analysis of impeller made of FV520B martensitic precipitated hardening stainless steel," *Engineering Failure Analysis*, vol. 34, pp. 501–510, 2013.

[26] N. Hrabe, T. Gnäupel-Herold, and T. Quinn, "Fatigue properties of a titanium alloy (Ti-6Al-4V) fabricated via electron beam melting (EBM): effects of internal defects and residual stress," *International Journal of Fatigue*, vol. 94, pp. 202–210, 2017.

[27] E. Malitckii, H. Remes, P. Lehto, Y. Yagodzinskyy, S. Bossuyt, and H. Hänninen, "Strain accumulation during microstructurally small fatigue crack propagation in bcc Fe-Cr ferritic stainless steel," *Acta Materialia*, vol. 144, pp. 51–59, 2018.

[28] C. Liu, Y. Liu, L. Ma, S. Li, X. Zhao, and Q. Wang, "Precipitate evolution and fatigue crack growth in creep and artificially aged aluminum alloy," *Metals*, vol. 8, no. 12, p. 1039, 2018.

[29] M. F. Moreira, "Failure analysis in aluminium turbocharger wheels," *Engineering Failure Analysis*, vol. 61, pp. 108–118, 2016.